JACS
JOURNAL OF THE AMERICAN CHEMICAL SOCIETY

Article

pubs.acs.org/JACS

Coinage-Metal Mediated Ring Opening of *cis*-1,2-Dimethoxycyclopropane: Trends from the Gold, Copper, and Silver Fischer Carbene Bond Strength

Laurent Batiste and Peter Chen*

Laboratorium für Organische Chemie, Eidgenössische Technische Hochschule (ETH Zürich), Vladimir-Prelog-Strasse 2, CH-8093 Zürich, Switzerland

Supporting Information

ABSTRACT: N-heterocyclic carbene (NHC) supported coinage metal cations proved to react in the gas phase with the electron-rich *cis*-1,2-dimethoxycyclopropane. Upon Collision Induced Dissociation (CID), several spectrometric fragment-ion signals were observed, one corresponding to the recovery of the bare cation IMes-M^+ (IMes = 1,3-bis(2,4,6-trimethylphenyl)imidazol-2-ylidene) and the second to the methoxymethylidene metal complex IMes−M−$[HCOCH_3]^+$. The gold and copper complexes appear to stabilize the carbene sufficiently enough to promote the latter channel. On the contrary, the silver complex binds weakly to the methoxymethylidene moiety as observed by the predominance of the bare cation IMes−M^+ channel. Density Functional Theory (DFT) investigations of the Potential Energy Surface and Bond Energy Decomposition Analyses provided results that correlate well with the experimental data. In the case of the bare cation channel, two distinct reaction pathways were found: a straightforward decoordination of the cyclopropane and a cationic rearrangement of the three-membered ring into a dimethoxypropylene isomer before dissociation. However, for the abstraction of the methoxymethylidene moiety by the metal cation, only one pathway was found. In analogy to earlier studies by other groups, we found the trend Au > Cu > Ag for the metal−carbene bond strength.

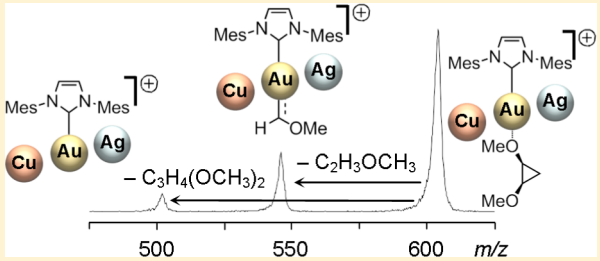

INTRODUCTION

The gas-phase synthesis of M−CH_2^+ species via the ring opening of cyclopropanes by transition-metal cations had been reported in the 1980s but remained limited to simple bare methylidene metal cations.[1] Threshold measurements for some of these gas-phase reactions, as well as for other metal−ligand bond dissociations, were subsequently performed.[1e−g] Recently, our group presented the mass-spectrometric synthesis of an IMes-supported Fischer Au(I) carbene generated from 1-ethoxy-2-methoxycyclopropane and IMes−Au^+ [IMes = 1,3-bis(2,4,6-trimethylphenyl)imidazole-2ylidene].[2] This reaction is an example of a gas-phase retro-cyclopropanation with a gold catalyst and was subsequently reported in solution by Echavarren's group for the gold-mediated benzylidene transfer from cycloheptatriene-norcaradiene species.[3] While Gassman reported the tungsten-mediated ring opening of cyclopropanes and metallocarbene formation as early as 1976,[4] the so-called retro-cyclopropanation had only been seen in solution for strained bicycle[1.10]-butanes reactions with Ni(0) and Rh(I) complexes.[5]

In order to understand why the Au(I) complex performs retro-cyclopropanation so readily, we decided to perform a study of bonding trends inspired in part from earlier Bond Energy Decomposition Analyses.[6] In analogy with our Au(I) chemistry, the isoleptic Cu(I) and Ag(I) complexes were probed, since we expected (possibly) similar gas-phase reactivity. Many coinage metal mediated carbene-transfer reactions have indeed been discovered in recent decades.[7] It appears, however, from the literature that Ag(I) in particular does not usually provide similar reactivity in insertion reactions or the decomposition of diazoesters into Fischer carbenes.[7b,8]

In addition to our previous report which provided a qualitative analysis of the gas-phase reactivity of dialkoxycyclopropanes with only IMes-Au^+ cations, the synthesis of the diastereomerically pure *cis*-1,2-dimethoxycyclopropane allowed the measurement of the energy barriers of the observed chemical processes by a quantitative Threshold Collision Induced Dissociation technique (TCID) for each specific coinage metal(I) complex. Mass spectrometry based on electrospray ionization and guided ion beam techniques in rf multipole ion guides is particularly powerful owing to its high sensitivity and ability to detect intermediate species of interest, even at low concentrations. We have used it to extract information on the mechanism and the barriers of catalytic reactions such as C−H bond activation,[9] reductive elimination,[10] transmetalation,[11] olefin metathesis,[12] and cyclopropanation.[2] Interpretation of the experimental results was assisted by the computation of the Potential Energy Surface (PES), for which we applied Density Functional Theory (DFT). Further

Received: August 19, 2013
Published: June 9, 2014

   dx.doi.org/10.1021/ja4084495 | *J. Am. Chem. Soc.* 2014, 136, 9296−9307

Scheme 1. Gas-Phase Synthesis and Fragmentation of Coinage Metal Complexes 3^{M}[a]

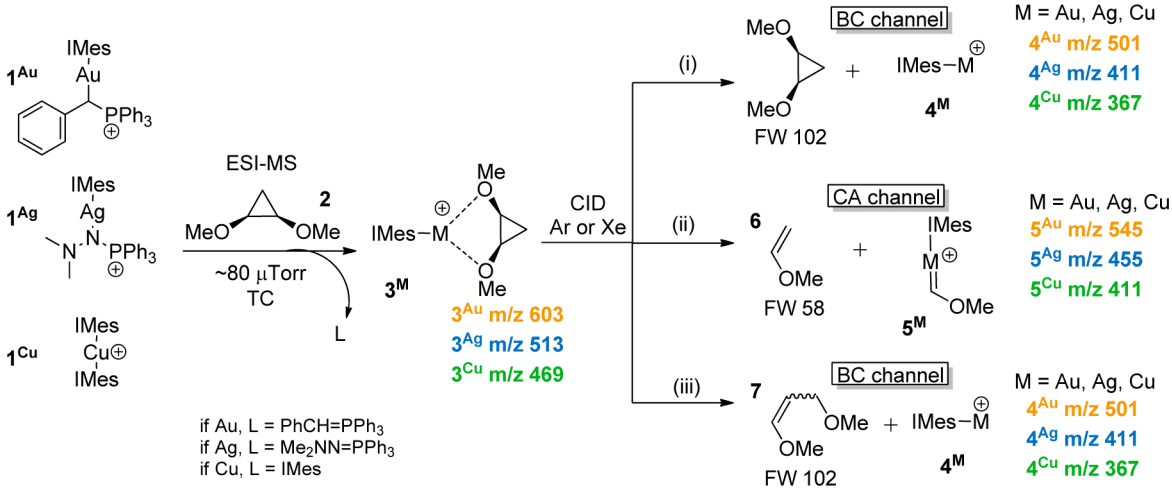

[a]The ions of interest, generated in the thermalization chamber (TC), were further mass-selected and underwent CID with xenon or argon. As discussed in the Results section, the carbene abstraction (CA) channel correspond to pathway (ii) while the bare cation (BC) channel can result from reactions along either pathway (i) or pathway (iii).

analysis, involving Bond Energy Decomposition Analysis, provided insight into the different interactions relevant to the metal−carbene bond strength and allowed us to establish a trend among the various metals.

METHODS

Mass Spectrometric (MS) Measurements. The energy resolved reaction cross section measurements were performed on a Finnigan MAT TSQ700 mass spectrometer equipped with a custom-made 24-pole ion guide as the first multipole.[10] Precursor cations $\mathbf{1}^{Cu}$, $\mathbf{1}^{Ag}$, or $\mathbf{1}^{Au}$ (Scheme 1) were generated by ESI from a 0.5 μM solution in 1,2-dichloroethane and were conducted into the thermalization chamber (TC) in which they collided under mild conditions with the reactant gas: *cis*-1,2-dimethoxycyclopropane **2** (see Supporting Information (SI) for synthesis). The soft collisions induced the dissociation of the labile ligand (**L**) and coordination of one molecule of *cis*-1,2-dimethoxycyclopropane, forming the ions of interest: $\mathbf{3}^{Cu}$, $\mathbf{3}^{Ag}$, and $\mathbf{3}^{Au}$. These ions were further mass-selected in the first quadrupole and underwent CID with argon or xenon gas. Finally the fragment ions[13] resulting from the CID channels were analyzed using a second quadrupole. For several equilibrated pressures of CID gas (set of 8 or 9 pressures from 20 to 110 μTorr), the fragmenting ion and fragment ion signal intensities were monitored over a certain range of voltage offsets, providing the so-called reaction cross sections. From the best energy-resolved cross sections, a calculated zero-pressure extrapolated curve was fitted with the L-CID program.[14] Subsequently, the thresholds E_0 for each channel were extracted from L-CID simulations and compared to DFT calculations. Each data set consisted of three independent runs composed typically of 15 individual fits. The variance of these fits was extracted from the Monte Carlo simulation in L-CID and was subsequently propagated by reciprocal variance-weighted averaging to obtain the variance for E_0.[10]

DFT Calculations. The calculation of the PES for all complexes was carried out first using the Gaussian 09 suite.[15] Geometry optimizations, harmonic frequencies, and the IRC studies were performed with the PW91,[16] mPW1K,[17] and M06-L functionals.[18] These functionals were chosen to model the various chemical processes such as ligand decoordination or transition-state paths (reaction kinetics) occurring in our chemistry. The meta-GGA functional M06-L was designed by Truhlar and co-workers[18] for transition metal complex thermochemistry and noncovalent interactions and is therefore suitable for representation of the various ligand−complex cleavages observed in the gas-phase experiments. On the other hand the mPW1K functional is claimed to be appropriate for reaction kinetics descriptions, i.e. activation barriers.[17] In an earlier study by our group also focused on gold carbenes chemistry,[2b] the PW91 functional gave good correlation with the experimental data. The calculations using these different DFT methods were performed for points of the PES pertinent for the reaction pathways. The inner electrons of Au, Ag, and Cu were described by two-component relativistic pseudopotentials.[19] The correlation-consistent, polarized double-ζ basis-set cc-pVDZ was used for the metals' valence electrons and for all electrons on other atoms (H, C, N, and O).[20] All structures reported here have been confirmed as stationary points on the PES using frequency calculations unless specified otherwise. Cartesian coordinates and absolute energies are available in the Supporting Information (SI). Extended Transition State Natural Orbitals for Chemical Valence bond analysis (ETS-NOCV),[21] as implemented in the Amsterdam Density Functional program package 2010 (ADF), was performed for the carbene intermediates on the M−C bond between the methoxymethylidene ($HCOCH_3$) and the IMes−M^+ moieties. This Bond Energy Decomposition Analysis provided some insight into the stabilization of the carbene moiety by the metal fragment. The latter analyses, the geometry optimizations, and the harmonic frequency calculations were performed with BP86[22] and a triple-ζ quality basis set augmented with one set of polarization functions. Scalar relativistic effects were considered for the transition metals using the zero-order regular approximation (ZORA).[23] Finally a screening of several density functionals was performed for the located intermediates and TSs with ADF using the Gaussian optimized PW91/cc-pVDZ(-PP) geometries and BP86/TZP densities (treatment of the relativistic effects with ZORA), in order to evaluate if another functional could perform better than the three functionals mentioned above.

RESULTS

Setting the Experimental Framework. In analogy to our previous study using 1-ethoxy-2-methoxycyclopropane,[2] the three coinage metal complexes IMes−M(I)−[1,2-dimethoxy-cyclopropane] $\mathbf{3}^{Cu}$, $\mathbf{3}^{Ag}$, and $\mathbf{3}^{Au}$ were formed in the thermalization chamber. Two CID channels were observed: (a) loss of 58 mass units (methylvinylether fragment **6**) which we assigned to the formation of the methoxymethylidene ($HCOCH_3$) metal(I) cation (pathway (ii), Scheme 1). In the present paper, we refer to it as the "carbene abstraction" channel (CA), and (b) loss of 102 mass units yielding the formation of the bare IMes−M^+ cation $\mathbf{4}^{M}$. The observation of the so-called "bare cation" channel (BC) can result from either

dx.doi.org/10.1021/ja4084495 | J. Am. Chem. Soc. 2014, 136, 9296−9307

fragmentation pathway (i) or (iii). Although the dissociation of the cyclopropane ligand (pathway (i), loss of cyclopropane **2**) appears to be the most straightforward rationale for the observation of this mass spectrometric signal, we also hypothesized, as will be justified in the Discussion section, that the "cyclopropane" moiety can undergo internal rearrangements before it dissociates (pathway (iii), loss of olefin **7**).

In the case of the Au series (Figure 1, yellow spectrum), the fragment ion signal related to the carbene abstraction (*m*/*z* 545) was the most intense. For the Cu series (Figure 1, green spectrum), the two fragment ion signals (*m*/*z* 411 and 367) were of comparable but low intensity. In the Ag series (Figure 1, blue spectrum), the carbene signal (*m*/*z* 455) was very weak, only rising up to 0.4% (relative intensity with 100 μTorr of xenon and −30.0 V offset) before it decreased in intensity when applying stronger voltage offset (see SI). Therefore, the latter channel could be neglected in a fit of the overall CID cross section; the fragmentation of $\mathbf{3}^{Ag}$ can be treated as a single channel situation. Based on these results, quantitative threshold measurements were performed so as to evaluate the activation barrier of the fragmentation channels observed upon CID of $\mathbf{3}^{Cu}$, $\mathbf{3}^{Ag}$, and $\mathbf{3}^{Au}$. The CID of $\mathbf{3}^{Ag}$ was carried out using xenon, whereas, for the measurements of $\mathbf{3}^{Cu}$ and $\mathbf{3}^{Au}$, argon was the gas of choice.[24]

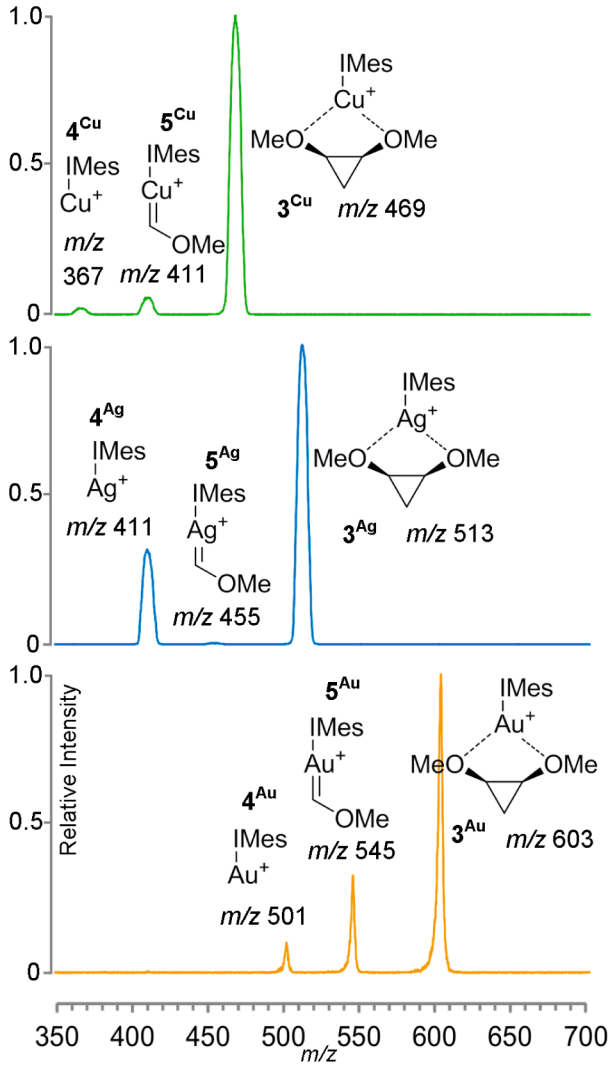

Figure 1. CID spectra of the [IMes−M−(*cis*-1,2-dimethoxycyclopropane)]$^+$ cations. Fragmentation pattern for $\mathbf{3}^{Cu}$, *m*/*z* = 469 obtained at −45.0 V voltage offset (Lab Frame Energy (E_{lab}), corresponding to a −3.45 eV Center-of-Mass Energy: E_{CM}) and 110 μTorr (argon). $\mathbf{3}^{Ag}$ *m*/*z* = 513 at −20.0 V (E_{CM} = −4.07 eV) and 100 μTorr (xenon). $\mathbf{3}^{Au}$ *m*/*z* = 603 at −60.0 V (E_{CM} = −3.73 eV) and 100 μTorr (argon).

L-CID Fits. A crucial aspect when setting the fitting criteria for L-CID was to determine the nature of the transition state model describing each channel.[14] A process in which the rate-determining step is an intramolecular rearrangement is treated as a "tight" transition state model.[10] On the other hand, if the rate-determining step corresponds to the final decoordination of an ion into two fragments, a "loose" transition state model applies. The E_0 values derived from the fits are necessarily model-dependent and, at this stage, should be treated as fit parameters. Whether they have a concrete physical interpretation depends on the degree to which the model is appropriate for the particular chemical system at hand. As will be later discussed and justified, the experimental curves related to the CA channel were fitted using the tight criterion for the Cu and Au series (the data for the CA channel in Ag were too low in intensity to be fitted with L-CID). The BC channel was fit with both a tight and loose transition state for Cu, Au, and Ag. These particular choices will be justified in the Discussion below.

The two reaction channels observed for the Cu series had low intensity, which made it hard to obtain high quality data. The L-CID fitting of their zero-pressure extrapolated cross sections was correspondingly difficult. The L-CID fit for the Cu data is furthermore performed only for center-of-mass collision energies below 3.4 eV because a third product channel appears at that energy (see SI), and L-CID is constructed to handle at most two observed channels. The activation energies for Cu have larger standard deviations (Table 1), but the curves themselves can still, in principle, provide chemically significant information regarding the mechanism. The Ag series benefited from cross section signals of high intensity for the single channel BC fragmentation which, after fitting, gave an energy barrier of 40.2 ± 1.3 kcal/mol. The Au series provided an intermediate case with a high intensity CA channel: 19.6 ± 0.8 kcal/mol; the low intensity BC channel gave an E_0 value estimated to be 52.2 ± 3.2 kcal/mol. As can be seen in Figure 2, the minor BC channel in Au contributes less than 10% to the total product cross section, which makes the fitted E_0 more uncertain for that channel than one might expect based on the statistical error bounds.

Table 1. L-CID Fitted Parameters in kcal/mol and Standard Deviations (in parentheses) of the Bare Cation (BC) and Carbene Abstraction (CA) Channels for Cu, Ag, and Au[a]

series	E_0^{BC}	E_0^{CA}
Cu	23.5 (1.5) t	44.8 (4.0) t
Ag	40.2 (1.3) l	–
Au	52.2 (3.2) l	19.6 (0.8) t

[a]LCID fits were performed based on assumption of a loose TS model (l) or a tight TS model (t).

Potential Energy Surface Analysis. Prompted in large part by the experimental CID results, the potential energy surfaces for the dissociation reactions, and the rearrangements with subsequent dissociations, were explored computationally. The metal−cyclopropane complex $\mathbf{3}^{M}$ was taken as the energy

dx.doi.org/10.1021/ja4084495 | J. Am. Chem. Soc. 2014, 136, 9296−9307

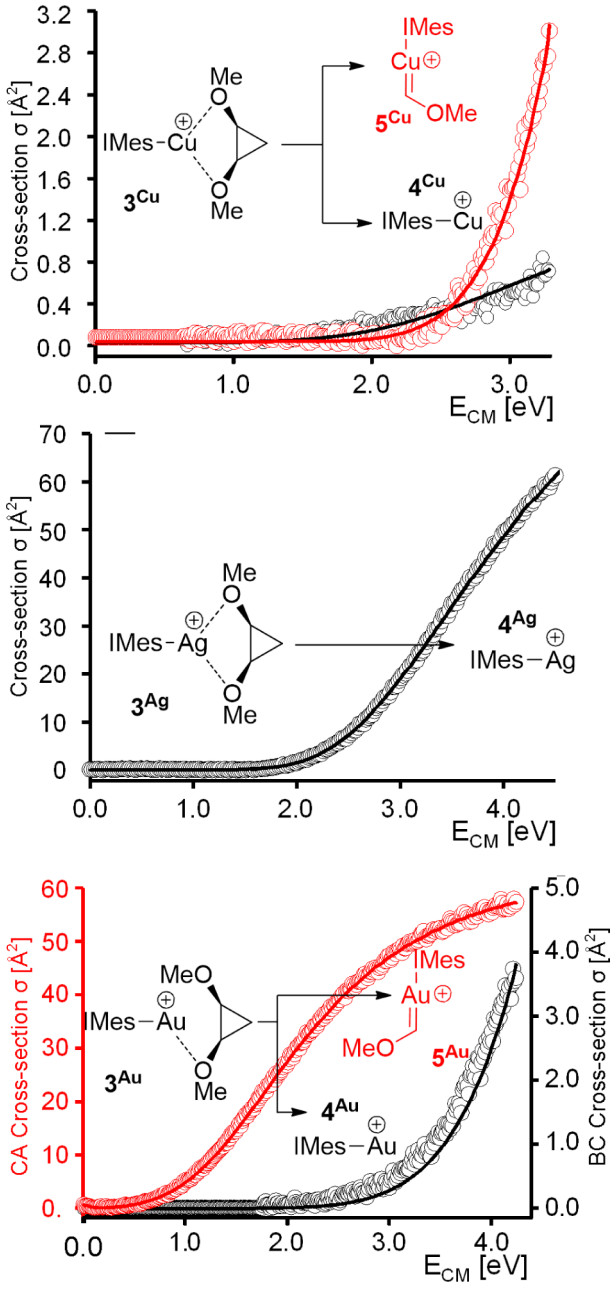

Figure 2. Zero pressure extrapolated cross sections for the Cu, Ag, and Au series (circles) and related L-CID fits (solid lines).

reference for the PES (PW91/cc-pVDZ(-PP)) since we assume that, after reaction with *cis*-1,2-dimethoxycyclopropane in the 24-pole and thermalization, the newly formed ions $\mathbf{3}^{M}$ did not further react before entering the CID chamber. From intermediate $\mathbf{3}^{M}$, three conceivable fragmentation pathways were investigated: the straightforward dissociation ((i), $\mathbf{3}^{M} \rightarrow \mathbf{4}^{M} + \mathbf{2}$ in Figure 3), the carbene abstraction ((ii), $\mathbf{3}^{M} \rightarrow \mathbf{5}^{M} + \mathbf{6}$ in Figure 3), and the H-shift and elimination ((iii), $\mathbf{3}^{M} \rightarrow \mathbf{4}^{M} + \mathbf{7}$ in Figure 4). Unless otherwise specified, the barriers and energies mentioned herein were computed with PW91/cc-pVDZ(-PP). The simple dissociation of the cyclopropane from the IMes−M^{+} moiety occurs through a loose barrier estimated to be around 40 kcal/mol for Au and Ag but above 48 kcal/mol for Cu. In our earlier report,[2a] we pointed out that the carbene abstraction pathway leading to the methoxymethylidene Au(I) species $\mathbf{5}^{M}$ (Figure 3) was rather complex. Despite our extensive investigations, a transition state directly connecting the reference $\mathbf{3}^{Au}$ to the "productive" carbocation $\mathbf{10}^{Au}$ could not be located. Access to $\mathbf{10}^{Au}$ eventually occurs after multiple internal displacements: ligand shift, ring opening, or ring closure ($\mathbf{TS}_{3-8}{}^{Au}$, $\mathbf{TS}_{8-9}{}^{Au}$, $\mathbf{TS}_{9-10}{}^{Au}$). Subsequently the carbocation $\mathbf{10}^{Au}$ undergoes lengthening of the central C−C bond ($\mathbf{TS}_{10-11}{}^{Au}$) over a low energy barrier (2.0 kcal/mol), yielding the π-stabilized Au(I)-methoxymethylidene $\mathbf{11}^{Au}$. The final dissociated state $\mathbf{5}^{Au}$ + **6** has an energy of 19.4 kcal/mol relative to the reference adduct and is 4.1 kcal/mol above $\mathbf{TS}_{9-10}{}^{Au}$. For the present work, geometry optimizations with PW91, mPW1K, and M06-L were carried out for intermediates $\mathbf{3}^{M}$, $\mathbf{4}^{M}$, $\mathbf{5}^{M}$, $\mathbf{10}^{M}$, $\mathbf{11}^{M}$ and Transition States $\mathbf{TS}_{9-10}{}^{M}$, $\mathbf{TS}_{10-11}{}^{M}$ for all three metals.[25] In contrast to the Au complex $\mathbf{3}^{Au}$, which is a linear bicoordinate complex, the structures $\mathbf{3}^{Cu}$ and $\mathbf{3}^{Ag}$ are tricoordinate, with the *cis*-1,2-dimethoxycyclopropane acting as an η^{2}-ligand. In addition, a direct path from complexes $\mathbf{3}^{Cu}$ and $\mathbf{3}^{Ag}$ to carbocations $\mathbf{10}^{Cu}$ and $\mathbf{10}^{Ag}$, respectively, was found and validated using the Intrinsic Reaction Coordinate method (IRC). The local barriers ($\mathbf{TS}_{3-10}{}^{Cu}$ and $\mathbf{TS}_{3-10}{}^{Ag}$) embodying the ring opening and formation of the single M−C σ-bond are 6.4 kcal/mol higher than the same barrier for gold. Similarly, the σ-coordinated carbocations $\mathbf{10}^{Cu}$ and $\mathbf{10}^{Ag}$ are more destabilized than their Au analogue. However, the second C−C bond cleavage ($\mathbf{TS}_{10-11}{}^{M}$) forming the unsaturated system of the ($HCOCH_3$) carbene proceeds over a 2.3 kcal/mol barrier for Cu; the corresponding barrier is 9.4 kcal/mol for Ag. With all DFT methods investigated in this study, the formation of the unsaturated system in the case of Ag requires a barrier at approximately 10 kcal/mol (see SI) and is usually higher in energy than for the two other metals. The asynchronicity of the three-membered ring opening, observed here, was also proposed to occur in the silver-mediated silylene transfer from silacyclopropanes to unsaturated systems.[26]

From the carbocation $\mathbf{10}^{M}$, which can be considered as a branching intermediate connecting several pathways on the potential energy surface,[2] the 1,3-hydride shift related to $\mathbf{TS}_{10-12}{}^{M}$ (Figure 4) results in the formation of the $\mathbf{12}^{M}$. The metallocarbene subsequently undergoes a concerted 1,2-hydride shift and elimination via $\mathbf{TS}_{12-13}{}^{M}$. After cleavage of the C−M bond, the π-complex $\mathbf{13}^{M}$ complex is formed, constituting the most stable intermediate on the potential energy surface for all three metals. A concerted transition state, connecting directly $\mathbf{10}^{M}$ to $\mathbf{13}^{M}$ via the hydride transfer from position 2 to 3 and elimination (see SI), lies higher in energy than the stepwise process.

Screening of Functionals. For a set of 75 DFT functionals, single-point calculations were performed for the highest barrier of each reported pathway. Although the inclusion of the *postfacto* dispersion correction (DFT-D)[27] seems to significantly improve the performance of most popular functionals, none of them performs better than PW91 (see SI).

Bond Energy Decomposition Analysis. We performed a Natural Orbitals for Chemical Valence bond analysis (NOCV)[21] for the M−C carbene bond between IMes−M^{+} and the ($HCOCH_3$) moieties in the complex $\mathbf{5}^{M}$. The evaluation of the σ and π contributions in the bond energy for each metal aimed at understanding the different behavior of silver that was observed experimentally and computationally. Among the bond decomposition analyses that have previously been performed on group 11 metal complexes, the studies on comparable systems[6,28] highlight the existence of the trend Au > Cu > Ag in term of bond strength.[6a,b] As can be observed in

dx.doi.org/10.1021/ja4084495 | J. Am. Chem. Soc. 2014, 136, 9296−9307

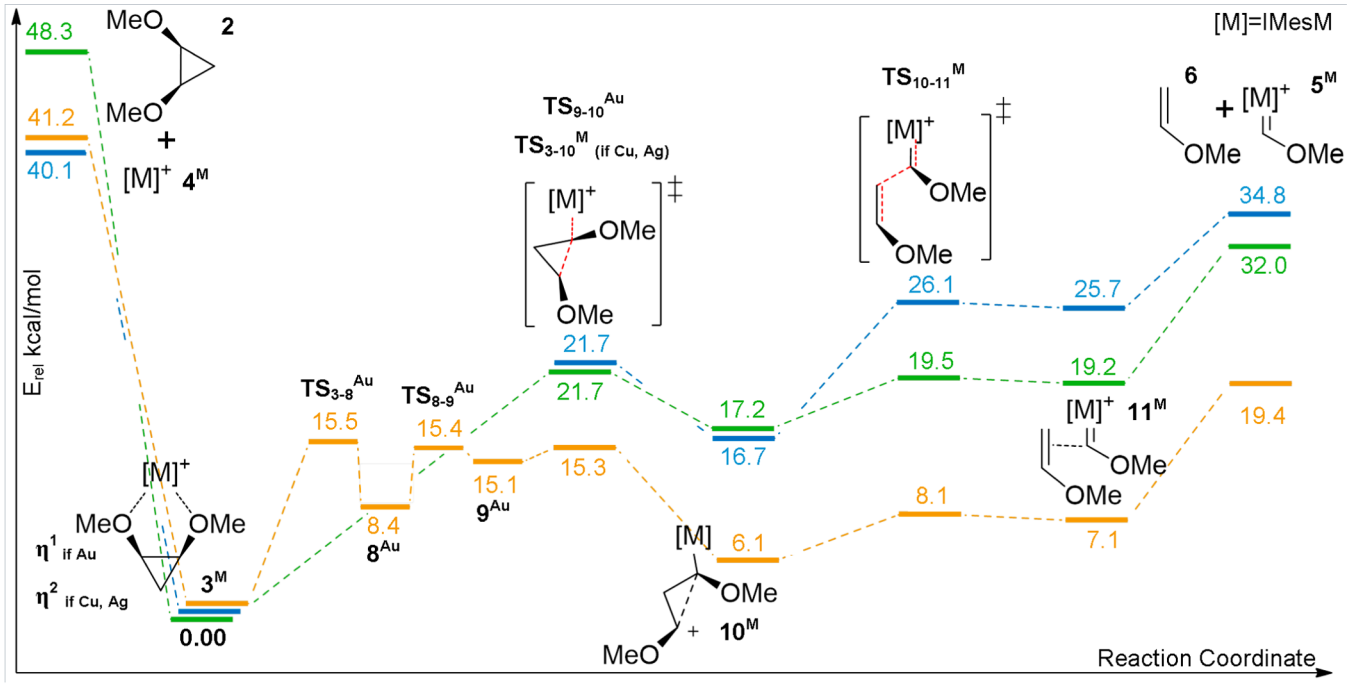

Figure 3. Zero-point energy (ZPE) corrected profiles with PW91/cc-pVDZ(-PP) from the reference structures 3^{Cu} (green), 3^{Ag} (blue), 3^{Au} (yellow) leading to the dissociation pathway (i) (4^{M} + **2**, left) or carbene abstraction pathway (ii) (5^{M} + **6**, right). Structures of $TS_{3-8}{}^{Au}$, 8^{Au}, $TS_{8-9}{}^{Au}$, and 9^{Au} were treated in detail in our earlier communication.[2]

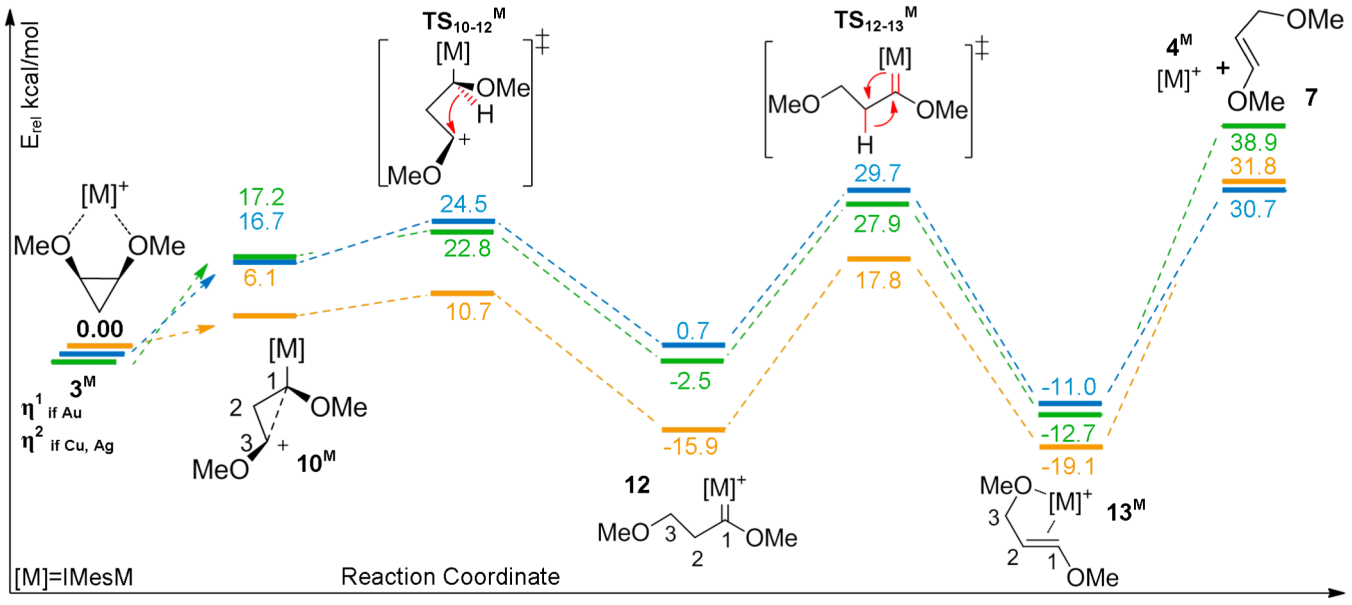

Figure 4. Zero-point energy (ZPE) corrected profiles with PW91/cc-pVDZ(-PP) leading to the H-shift-elimination pathway (iii) (4^{M} + **7**). From the structures 3^{Cu} (green), 3^{Ag} (blue), 3^{Au} (yellow) to the corresponding carbocations 10^{Cu}, 10^{Ag}, and 10^{Au}, the PES is the same as reported in Figure 3.

Table 2, a similar order was found in regard to the net bonding energy (ΔE_{Net}). The Bond Energy Decomposition Analysis shows that the electrostatic interaction ΔE_{elstat} contributes in a much larger proportion to the stabilization of the bond system (about 70%) than the covalent interaction (i.e., orbital contribution ΔE_{oi}). Frenking and co-workers reported energy decomposition analyses with a similar prevalence of the electrostatic factor from 60% to 75% in η^1-allene or carbonyl gold complexes.[29] More specifically the gold system exhibits a much stronger electrostatic interaction (−208.8 kcal/mol) than copper and silver (−146.9 and −141.3 kcal/mol respectively), which is partly counterbalanced by gold's very large Pauli repulsion. The Bond Energy Decomposition Analysis indicates four significant orbital interaction energy contributions which were assigned to various sorts of σ- or π-components. The σ-type donation from the ($HCOCH_3$) fragment into the metal center dominates with between 50 and 60% of the overall orbital interaction. A depletion of electron density (see orange surface in Figure 5) is observed from the ($HCOCH_3$) carbene area while a gain of electron density (green) occurs in the bonding area between the metal and the carbene fragments. Subsequently a slight gain in electron density is observed on the

dx.doi.org/10.1021/ja4084495 | J. Am. Chem. Soc. 2014, 136, 9296−9307

Table 2. Bond Energy Decomposition Analysis of the M−C Bond in ($HCOCH_3$) Carbene Complexes 5^{Cu}, 5^{Ag}, and 5^{Au} in kcal/mol and Indicative Bond Distances

	Cu		Ag		Au	
ΔE_{int}	−75.91		−58.59		−82.02	
Steric Int	−21.96		−14.53		−6.82	
ΔE_{Pauli}	124.9		126.8		201.95	
ΔE_{elstat}	−146.86	73.1[a]	−141.3	76.2[a]	−208.77	73.5[a]
ΔE_{oi}	−53.95	26.9[a]	−44.06	23.8[a]	−75.2	26.5[a]
σ-don.	−26.42	49.0[b]	−23.78	54.0[b]	−43.45	57.8[b]
$\pi_\perp$-backdon.	−16.05	29.7[b]	−8.66	19.7[b]	−16.33	21.7[b]
$\pi_\parallel$-backdon.	−4.88	16.7[b]	−4.96	18.9[b]	−6.26	15.8[b]
π/σ-backdon.	−4.11		−3.38		−5.62	
$Rest_{oi}$	−6.60		−6.66		−9.15	
ΔE_{Prep}	5.14		1.53		6.45	
Fragment M−IMes	0.83		0.19		1.79	
Fragment $HCOCH_3$	4.31		1.34		4.66	
ΔE_{Net}	−70.77		−57.06		−75.57	
$M-C_{IMes}$[c]	1.897		2.092		2.045	
$M-C_{HCOMe}$	1.85		2.071		1.986	
C−O	1.296		1.288		1.292	

[a]% of the overall bond stabilization. [b]% of the covalent contribution. [c]Bond distances in Å. The steric interactions (Steric Int) component is the sum of the Pauli repulsion (ΔE_{Pauli}) and electrostatic attraction energies (ΔE_{elstat}).

IMes carbene area which ensues from the weakening of this $M-C_{IMes}$ bond. As reported in the literature, the stabilization through the σ-component is more important for gold (−43.5 kcal/mol, Table 2) than for the two other metals (∼ −25 kcal/mol). Among the π-type interactions along the M−C bond, only the out-of-plane $\pi_\perp$ contributions of the IMes and ($HCOCH_3$) carbenes were considered (Figure 6).[30] Indeed only such overlap allows the empty p orbital of the carbene moiety to be filled. In this regard, both copper and gold systems benefit from a better stabilization than silver for $\pi_\perp$ interactions (−16.05, −16.33 kcal/mol, respectively, in comparison to only −8.66 kcal/mol). In contrast, the in-plane $\pi_\parallel$ interactions are unimportant as they populate the antibonding orbitals σ^* of the C−O and C−H on the ($HCOCH_3$) moiety.

DISCUSSION

The specific motivation for this work is the comparison of the retro-cyclopropanation reaction, which here is designated CA. The observation of additional product channels complicates the extraction of thresholds for the CA channel, but a careful analysis of the data with the DFT calculations does nevertheless provide chemically useful information. Each of the CID threshold experiments shown in Figure 2 includes, in principle, a competition between two (or more) fragmentation channels. The L-CID program was structured to handle up to two competing product-forming channels. We detect product formation by mass spectrometry, which necessarily means that a given product channel becomes visible only in the case that it ends in a dissociation, which changes the m/z ratio. Each of the individual channels can furthermore proceed via multiple steps, with multiple transition states. Assigning the E_0 fit parameters to a chemically meaningful event is straightforward for a simple dissociation without prior rearrangement, which

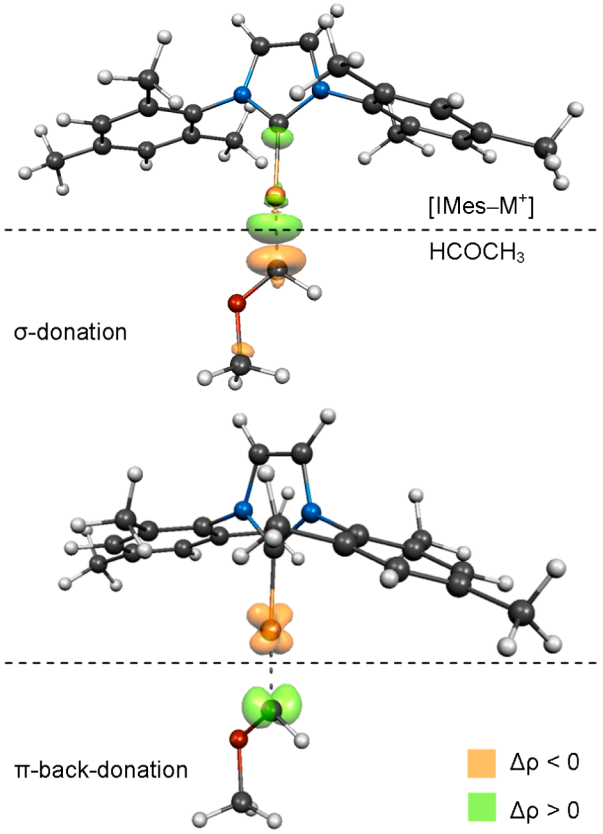

Figure 5. Dominant σ-type and π-type orbital interaction energy contributions in the Bond Energy Decomposition Analysis for 5^{Cu}. The σ-contribution is characterized by a depletion of electron density (orange) from an sp^x orbital on carbene and a gain (green) in the M−C bonding area. The π-contribution corresponds to the transfer of electron density from the metal d orbital into the carbon p orbital.

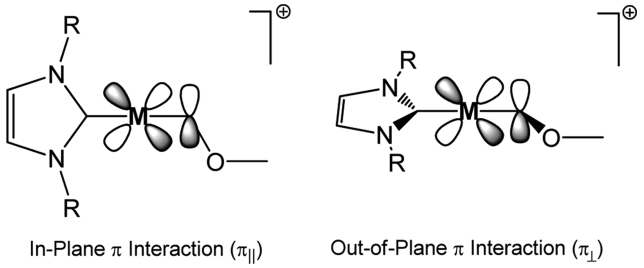

Figure 6. In-plane and out-of-plane π-interactions along the M−C carbene bond.

comprises the simplest case for our experiment. A pathway with multiple steps, however, can be much more complicated. As internal energy increases, the density of states grows more quickly for loose transition states than for tight transition states. Consequently, the reaction rate of a loose process is more accelerated by the increase of the internal energy than the rate of a tight process. Figure 7 presents the generalized case of the fragmentation of an ion **A** into its fragment ion **C** and neutral **D** via an intramolecular rearrangement with a given barrier (**A** → **B**) and dissociation (**B** → **C** + **D**) with a slightly higher barrier. Based on Rice-Ramsperger-Kassel-Marcus (RRKM) theory, at the onset of the overall process (area 1 in red), the kinetics of the composite process (**A** → **C** + **D**) is limited by the rate of dissociation (red dashed line). As the collision energy is raised, the rate of transit over the tight barrier (blue dashed line) is less

dx.doi.org/10.1021/ja4084495 | J. Am. Chem. Soc. 2014, 136, 9296−9307

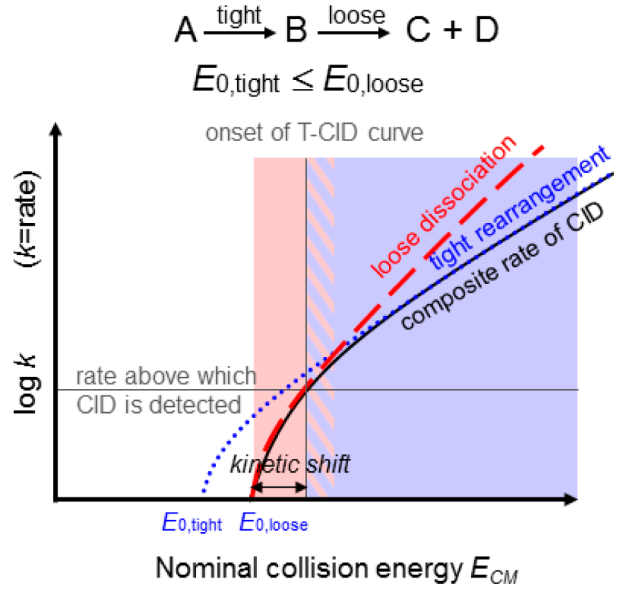

Figure 7. Schematic representation of the generalized RRKM rates for the internal (tight) rearrangement of **A** to **B** and the subsequent more endothermic loose dissociation to **C** and **D**. For area 1, near the onset, $k_{overall}$ is dominated by the loose dissociation. At higher energy (area 2), the tight barrier is the RDS.

accelerated than the rate of dissociation until the tight process (**A** → **B**) becomes the rate-determining step (area 2 in blue). Considering, though, the kinetic shift in the process, **A** → **C** + **D**, makes the argument more complicated. Upon collisional activation, a rapid and statistical redistribution of the energy along all vibrational modes (degrees of freedom) occurs prior to the fragmentation of the ion. Because the experiment observes a dissociation only when the (microcanonical) rate rises above a finite threshold determined by the spectrometer, the dissociation becomes observable only at some energy above E_0. The difference is the kinetic shift, marked in Figure 7. For molecules with 50−100 atoms, the kinetic shift is large enough so that, typically, as shown in Figure 7, the observed onset of the cross section curves is already in a range of collisional energy (blue area) where the kinetics are governed by the rate of transit over the tight barrier.[10] Such complex features were encountered in earlier work;[2b,11b] the experimental cross sections were fitted with L-CID using a tight TS model because most of the data points in the CID cross section were in area 2, significantly above the onset, with the kinetics governed unambiguously by the rate of transit over the tight barrier. In practice, for molecules with 50−100 atoms in our spectrometer, a loose transition state for **B** → **C** + **D** needs to be at least 15−20 kcal/mol higher than the tight transition state for **A** → **B** before the loose transition state becomes rate-limiting over the several eV range of our T-CID measurement.

Referring now to Scheme 1, the pathways labeled (ii) and (iii) involve internal rearrangements (for instance $\mathbf{TS}_{3-10}^{M}$ and $\mathbf{TS}_{12-13}^{M}$) that are, in our cases, close enough in energy to the final dissociation asymptotes and therefore should affect the reaction kinetics. More specifically, the final dissociation asymptotes for the channels corresponding to (ii) and (iii) in Scheme 1 are computed to lie only 19−35 kcal/mol above the starting complexes, while the internal tight transition states lie around 10−20 kcal/mol, and hence less than 15−20 kcal/mol below the loose transition states for subsequent dissociation. When fitting the related experimental cross sections with L-CID, based on the above discussion, a tight model will be used, as depicted in Figure 7. Channel (i) in Scheme 1 is a simple dissociation with no preceding rearrangement, so it can be treated with a loose model.

Having made this didactic digression, we now return to the threshold CID experiments in Figure 2. As mentioned, each of the three experiments involves, in principle, a competition between the BC (without rearrangement) channel, which corresponds to pathway (i) in Scheme 1, the CA channel, pathway (ii), and the BC (with rearrangement) channel, which is pathway (iii). Even though the calculations of the PES indicate that pathway (i) looks to be energetically disfavored, the simple dissociation through a loose transtion state should be kinetically competitive with competing processes whose rate-limiting tight transition states are 15−20 kcal/mol lower in energy (approximately). Therefore, even before a comparison of the experimental results to the calculated potential energy surfaces, the shapes and appearance of the threshold CID curves for the Cu, Ag, and Au systems reveal gross features of the chemistry of $\mathbf{3}^{M}$.

The simplest interpretation comes for $\mathbf{3}^{Ag}$, which shows only one significant product channel, the BC channel. There is a very small peak corresponding to the CA channel, never exceeding 0.4% in relative intensity. Not only is a fit for this channel not possible (statistically), but its inclusion makes no difference in the E_0 value derived for the main BC product channel. The CID of $\mathbf{3}^{Ag}$ is therefore treated as a single channel process.

Next in complexity comes $\mathbf{3}^{Au}$, for which there are two product channels, CA and BC, with the CA channel comprising >90% of the product cross section. The dominant CA channel, which involves multiple high energy internal rearrangements (and should therefore be fitted using a tight transition state model), has its onset at a lower energy than does the BC channel, and its more than 10-fold higher cross section means that a fit with L-CID should produce a reliable E_0 with a clean chemical interpretation. For the competing, low-intensity BC channel, fits with either a loose transition state (straightforward dissociation, pathway (i)) or a tight transition state (H-shift and elimination, pathway (iii)) give higher E_0 values with "looser" transition states, which would explain why the minor channel is competitive at all at higher collision energies.

The most difficult-to-interpret shapes occur for $\mathbf{3}^{Cu}$. The BC channel has a low energy onset, but rises very slowly. The competing CA channel starts at a higher E_0 but rises rapidly, overtaking the BC channel. Keeping in mind that the CA channel proceeds via a rate-limiting tight transition state and its onset is higher in energy than that for the BC channel, one necessarily concludes that the BC channel cannot proceed via a rate-limiting loose transition state. More concretely, if one were to assume that the BC channel proceeds as a simple dissociation through a loose transition state, then its lower energy onset would mean that a CA channel with higher E_0 and tight transition state should never be observable. It would never become kinetically competitive, which stands obviously at odds with the experimental curves. Accordingly, one can argue from the gross shape of the curves for $\mathbf{3}^{Cu}$ that the BC channel cannot proceed via a loose transition state, at least not over the entire energy range.

From the chemical point of view, we had initially treated the BC channel as a simple dissociation of $\mathbf{3}^{Cu}$ into $\mathbf{4}^{Cu}$ and **2**: the observed (IMes)Cu^+ ion and *cis*-1,2-dimethoxycyclopropane, respectively. However, the latter fragment **2** is mass spectro-

dx.doi.org/10.1021/ja4084495 | J. Am. Chem. Soc. 2014, 136, 9296−9307

metrically invisible because it is uncharged. In considering explanations for the threshold CID curves, one should recall that there is no independent evidence that the neutral fragment is, in fact, *cis*-1,2-dimethoxycyclopropane rather than a valence isomer of the same composition, and, hence, the same mass. A rearrangement along the reaction coordinate of the BC channel can, in principle, proceed by a rate-limiting tight transition state—one of the rearrangement steps—as long as the final dissociation to $\mathbf{4}^{Cu}$ and a lower energy valence isomer of *cis*-1,2-dimethoxycyclopropane is faster than the straightforward dissociation which we postulate for the Ag and Au cases. This possibility appears to be the only reasonable explanation for the shape of the threshold CID curves for $\mathbf{3}^{Cu}$. Accordingly, we performed an L-CID fit under these assumptions, which, by themselves, do not depend on L-CID but rather on general considerations of competitive reactions. We then initiated an extensive computational search for a suitable rearrangement which would be consistent with the shape of the experimental curves, which ultimately led to the appropriate pathway, depicted in Figure 4. The alternative pathway, designated as (iii) in Scheme 1, involves the rearrangement of the *cis*-1,2-dimethoxycyclopropane into the *E*-1,3-dimethoxypropylene, a lower energy isomer, via a series of internal rearrangements of high energy and final dissociation from the bare cation $\mathbf{4}^{Cu}$. The consequence would be the use of a tight transition state model for the fit of the BC channel in the Cu case.

Having qualitatively interpreted the experimental curves, we can now correlate the quantitative threshold measurements with the DFT calculated barriers. In the Ag series, the quantitative measurements for the single BC channel estimated this loose barrier at 40.2 ± 1.3 kcal/mol. Considering the PW91/cc-pVDZ(-PP) computed energies, the dissociation pathway ($\mathbf{3}^{Ag} \rightarrow \mathbf{4}^{Ag} + \mathbf{2}$) proceeds in one step with the computed barrier of 40.1 kcal/mol, in very good agreement with the experimental threshold measurement, although this degree of agreement is probably fortuitous. Examining the potential energy surface for Ag in Figure 3 reveals that the straightforward dissociation is computed to have a rate-limiting loose barrier of 40.1 kcal/mol, which is lower than the corresponding barrier for Cu or Au. Looking at the BC channel with rearrangement, Figure 4, one sees that Ag would have a tight transition state at 29.7 kcal/mol for the intramolecular H-shift, the highest value among the three metals, which, while just slightly lower than the dissociation asymptote of 30.7 kcal/mol, would certainly be rate-limiting for that BC channel with rearrangement (iii). It is therefore likely that the BC channel with rearrangement would not be kinetically competitive against the straightforward dissociation, indicating that the proper choice of transition state model for an L-CID fit would be loose. A test with a fit of the same BC channel data to a tight transition state model gives 24.5 kcal/mol (see SI). One could argue this result is consistent with the calculated barriers with PW91. Such a conclusion however implies that the CA channel should then have significant intensity as well. The CA pathway in Ag ($\mathbf{3}^{Ag} \rightarrow \mathbf{5}^{Ag} + \mathbf{6}$ (i)) is indeed computed to be endothermic by 34.8 kcal/mol and involves tight internal rearrangements of similar height as in the case of pathway (iii). It however never exceeds 0.4% of the highest peak intensity (and 0.8% of the BC channel intensity). We would therefore expect similar behavior for the BC channel with rearrangement. The details of the computed PES for Ag are accordingly consistent with the expectations derived from the experimental CID curves.

Similarly a good correlation is found with the PES around $\mathbf{3}^{Au}$ for the CA channel. The carbene abstraction pathway ($\mathbf{3}^{Au} \rightarrow \mathbf{5}^{Au} + \mathbf{6}$) is 21.7 kcal/mol less endothermic than the loose dissociation pathway ($\mathbf{3}^{Au} \rightarrow \mathbf{4}^{Au} + \mathbf{2}$), which is consistent with the qualitative analysis in the preceding paragraphs of the Discussion. Our threshold measurements give results with a small standard deviation for the CA energy barrier (19.6 ± 0.8 kcal/mol), which agrees well with what we found with the PW91-computed PES in which several intramolecular rearrangements with (tight) barriers in the 15−16 kcal range are followed by a final dissociation with a (loose) barrier of 19.4 kcal/mol. For the (barely) competing BC channel, a straightforward dissociation pathway ($\mathbf{3}^{Au} \rightarrow \mathbf{4}^{Au} + \mathbf{2}$) could account for observation of the mass spectrometric signal *m*/*z* 501 that starts rising at higher energy. The low intensity curves obtained for this channel made the L-CID fits less accurate. A dissociation barrier, assuming a loose transition state, would be 52.2 kcal/mol with a high standard deviation of 3.4 kcal/mol derived from the statistical analysis of the fit. The match to the computed activation energy, 41.2 kcal/mol calculated with PW91/cc-pVDZ(-PP), is poor, but with the low intensity of the signal in this channel and the attendant difficulties in the fit, the difference can be rationalized. The alternative for the minor channel would correspond to a fit with a tight transition state, from which the E_0 value of 37.2 kcal/mol (see SI) is derived. Whether pathway (iii) is ever competitive against pathway (ii) for Au is questionable, based on the computed potential surfaces, but we cannot exclude the possibility definitively. Accordingly, the experimental data, even combined with the computations, do not provide a clear diagnostic as to the nature of the minor channel in the case of Au. Given that this channel accounts for <10% of the product cross section, and given that the motivation for the present work concerns the CA channel, this ambiguity remains, but has little consequence. Additionally fitting the CA channel with a tight TS model provides similar results (19.6 and 20.0 kcal/mol; see SI) independently of whether the BC channel is treated with a tight or loose TS model.

As we foresaw from the qualitative analysis of the cross section curves, the calculations suggest for Cu that the BC channel is the composite of two distinct reactions, namely the dissociation pathway ($\mathbf{3}^{Cu} \rightarrow \mathbf{4}^{Cu} + \mathbf{2}$) and the *H*-shift-elimination pathway ($\mathbf{3}^{Cu} \rightarrow \mathbf{4}^{Cu} + 7$). With PW91, the single-step dissociation would proceed over a rate-determining loose TS at 48.3 kcal/mol. The carbene abstraction pathway ($\mathbf{3}^{Cu} \rightarrow \mathbf{5}^{Cu} + \mathbf{6}$) and the H-shift-elimination pathway ($\mathbf{3}^{Cu} \rightarrow \mathbf{4}^{Cu} + 7$) are endothermic by 32.0 and 38.9 kcal/mol, respectively. As noted for fragmentation of $\mathbf{3}^{Au}$ and $\mathbf{3}^{Ag}$, the tight internal rearrangements of these two pathways are rate-determining at high internal energy. For low collision energy, the carbene abstraction pathway and the *H*-shift-elimination pathway may account for the observation of signals *m*/*z* 411 and 367, respectively. As the collision energy is raised, the contribution of the internal rearrangements in the reaction rates increases. Consequently, the *H*-shift-elimination pathway is disfavored because of the high lying $\mathbf{TS}_{10-12}{}^{Cu}$ and $\mathbf{TS}_{12-13}{}^{Cu}$, whereas the carbene abstraction pathway displays no barrier from $\mathbf{10}^{Cu}$ to $\mathbf{5}^{Cu} + \mathbf{6}$ except the final dissociation and therefore evolves into the preferred pathway. Lastly at higher collision energy, the dissociation pathway ($\mathbf{3}^{Cu} \rightarrow \mathbf{4}^{Cu} + \mathbf{2}$) becomes accessible and should account for a large part of the intensity of signal *m*/*z* 367 (BC channel). Due to the existence of two independent pathways in the BC channel, the L-CID fits for Cu are difficult

dx.doi.org/10.1021/ja4084495 | J. Am. Chem. Soc. 2014, 136, 9296−9307

to correlate to the calculated PES. Moreover the low intensity of the cross section curves in the possible range of collision energy leads to a poor signal-to-noise ratio and a less-than-optimal zero-pressure extrapolation. Indeed the CA-channel curve starts rising later than the BC channel, and a slight dipping under the zero-value can be observed (see SI). Due to the contribution of two reaction pathways to one spectrometric signal (BC channel), the measurement correlates neither wholly with the dissociation pathway (i) nor entirely with the H-shift-elimination pathway (iii). Aside from the conclusion that the DFT calculations render it plausible that the BC channel is a composite of pathways (i) and (iii), which is a nevertheless useful conclusion, the assignment of the fitted E_0 value to a single chemical process is most probably not a fruitful exercise. Because the fitting for what the DFT calculations suggest is a three-channel problem was done for two observed product channels (pathways (i) and (iii) producing an observed product with the same m/z ratio), it is not completely clear how meaningful E_0 for the CA channel should be. On the other hand, the CA channel constitutes over 80% of the total product cross section at the higher energies in Figure 2. The appearance of yet another product channel above 3.4 eV limited the range of collision energies for the fit, but one may nevertheless argue that the extracted E_0 value is meaningful. E_0 for the CA channel, 44.8 ± 4.0 kcal/mol, is not too far from the overall calculated barrier for the carbene abstraction pathway (32.0 kcal/mol). While the quantitative comparison of E_0 values to the computed PES for the Ag and Au cases gives encouragingly good agreement in several points, the Cu experiment is less informative in this regard. Nevertheless, as noted before, the gross shape of the CID curves for Cu motivated a much more extensive computational search for alternative product channels, which was fruitful. The resultant PES for Cu does, in fact, render what had otherwise been an ad hoc explanation for the CID curves plausible.

In summary, the fitting results agree to a satisfactory extent with PW91/cc-pVDZ(-PP) barriers. The Perdew–Wang exchange-correlation functional therefore seems to be adequate for at least a qualitative description of the experimentally observed features of this system, as it has been already remarked in our previous studies.[6,35] The calculated barriers for the dissociation pathway (i) using the M06-L or mPW1K functional also agree with the fitted energies acceptably, while those for the pathways (ii) and (iii) are higher (see SI).

Having obtained the E_0 values for various processes by L-CID fitting of the experimental threshold curves, and having identified the most probable rate-limiting transition states by comparison to DFT calculations of the potential surface, we return to a top-level view of the overall chemistry of the Cu, Ag, Au series of complexes, especially with regard to the CA channel which motivated the comparison in the first place. Even a cursory examination of the CID behavior of the three species, $\mathbf{3}^{Cu}$, $\mathbf{3}^{Ag}$, and $\mathbf{3}^{Au}$ shows that the reactivities of Cu and Au resemble each other, at least in the gross features of the cyclopropanation and retro-cyclopropanation reaction, while the reactivity of Ag is different. In particular, we find that $(IMes)Cu^+$ and $(IMes)Au^+$ can abstract a carbene unit from electron-rich cyclopropanes in the gas phase. $(IMes)Ag^+$ cannot, or at least not with a comparable efficiency. Considering the particular pattern of Au > Cu > Ag, the most important determinant of the gross features of the CID behavior of $\mathbf{3}^{M}$ is thermochemical. Take the equation:

$$(IMes)M^+ + \textit{cis}\text{-}1,2\text{-dimethoxycyclopropane} \rightarrow [(IMes)M(HCOCH_3)]^+ + \text{methylvinylether}$$

The net change in the reaction can be summarized as a loss of two C–C σ-bonds against a gain of a C–C π-bond plus the M–C bond. For the Cu, Ag, and Au series, the only difference would then be the strength of the M–C bond in the carbene complex. While, in the comparable case of the nitrene complexes,[6f] the metal–nitrogen bond strength could be measured directly by CID of the metal aminonitrene complexes themselves, the analogous metal–carbon bond strengths are not experimentally accessible in the same way. A direct cleavage of the stronger M–C bond is problematic because the higher threshold makes it more likely that there will be intervening side reactions. The present experiment, with the retro-cyclopropanation, provides effectively a measure of the metal–carbon bond strength, albeit indirectly. Accordingly, the retro-cyclopropanation reaction, the immediate object of the present study, becomes a surrogate for a different experiment, which, together with the earlier metal nitrene study, tells a more general story of trends in bonding for the coinage metals. Earlier studies by Armentrout and Beauchamp[1] have found periodic trends in bond strengths with which our observed trends are consistent. Namely the gold and copper $M^+–H$, $M^+–CH_3$, and $M^+–CH_2$ complexes appear much more strongly bound than the silver ones. Interestingly enough, the dissociation energy for complexes of the type $M^+–CH_3$ reveals the greater propensity of gold in σ-bonding.[1g–i] Additionally, a 36.2 kcal/mol increment in bond strengths was observed when switching from the $M^+–CH_3$ to $M^+–CH_2$ system for both copper and gold (in all cases, the silver–carbon bond appears much weaker). Such an observation is again consistent with our Bond Energy Decomposition Analyses where the π-contribution of both copper and gold are of similar magnitude. With M06-L, which was specifically designed by Truhlar's group to treat metal–ligand bond strengths, the dissociation energy from the metal-coordinated to the free methoxymethylidene species is calculated to be around 70 kcal/mol for both the Cu(I) and the Au(I) carbenes (Table 3). In contrast silver appears to stabilize the methoxymethylidene moiety less efficiently. Furthermore, the estimates of the energies with PW91 follow the same trend but suggest a better stabilization by gold (77.9 kcal/mol) compared to copper (72.5 kcal/mol). The latter results seem more in agreement with our experimental observations and confirm the suitability of the PW91 functional in describing our system. In any case, the same gross trend in bond strengths is reproduced here for all DFT methods investigated. The H–C–O angles reveal that the methoxymethylidene silver (105°) tends more toward the free-carbene form (100°) than its copper (112°) or gold (113°) analogues (PW91 functional; see SI).

Table 3. Bond Energies for the Metal–Carbon Bond Dissociation of the Methoxymethylidene Metal Complexes with M06-L, PW91, and mPW1K in kcal/mol

	M06-L	mPW1K	PW91
Au	70.6	55.3	77.9
Cu	69.7	42.3	72.5
Ag	56.5	34.0	61.4

The trend Au > Cu > Ag in the metal–carbon bond strengths having been shown, we now aim at examining the

dx.doi.org/10.1021/ja4084495 | J. Am. Chem. Soc. 2014, 136, 9296–9307

origins of the pattern. To construct a crude strawman explanation, one might have expected that the bond energies of the coinage metal centers to first-row elements such as C or N might vary monotonically, with the bond getting weaker as one goes down a column. The principal quantum number of the occupied orbitals in the valence shell of the metal increases going down the column, which might lead one to expect that both the overlap and energy gap to *2s* and *2p* orbitals on carbon or nitrogen would be adversely affected. The naïve expectation, however, is quickly dispelled by an examination of periodic trends in various physical properties, which have been systematized as consequences of the strong relativistic effects, particularly for gold.[31] Nevertheless, going from the general case to the specific bonding situation in $[(IMes)M(HCOCH_3)]^+$, the Bond Energy Decomposition Analysis provides a basis from which one can understand which interactions produce the trend Au > Cu > Ag in bond strengths. In light of the Bond Energy Decomposition Analysis results where the σ-contribution in $\mathbf{5^M}$ is twice as big for gold (−43.5 kcal/mol) as for copper and silver (∼ −25 kcal/mol), one can suppose that, also for complex $\mathbf{10^M}$, the [IMes−Au] moiety provides a better σ-stabilization. The unusually large relativistic *6s* orbital contraction and its resulting energy lowering produce a stronger electron acceptor ability of Au(I) and a better orbital interaction.[32] Consequently the barrier for ring opening and the first M−C single bond formation is much lower for gold than for the two other metals. The strong Lewis acidity of monodentate Au(I) complexes,[33] viewed as otherwise analogous to H^+, may also explain the ease in ring opening of cyclopropanes as observed for protonated cyclopropane $C_3H_7^+$.[34] This peculiarity of gold has been further exploited in the synthesis of *gem*-diaurated compounds.[35] It is important to point out here that even though the gold carbene displays the greatest orbital interactions, notably because of the strong σ-bonding, the overall stabilizing interaction between the carbene moiety and the metal center is almost as high for copper since it compensates its weaker covalent bond by a stronger electrostatic interaction (as can be seen in the Steric Int component in Table 2).

In the last step of the retro-cyclopropanation, the C−C bond cleavage results in the formation of a vacant *p* orbital on the carbon of the carbene moiety. Therefore, the stabilization of this low lying unoccupied *p* orbital by π-back-donation from the metal *d* orbitals is crucial for keeping a low energy barrier.

According to the Bond Energy Decomposition Analysis, such stabilization is significant for copper and gold, particularly the out-of-plane π-contribution (−16.05 and −16.33 kcal/mol respectively) which involves a direct overlap with the empty *p* orbital. However, the Ag(I) carbene exhibits a weaker π-back-donation which leads to a high barrier from $\mathbf{10^{Ag}}$ to $\mathbf{TS_{10-11}^{Ag}}$ where the π-system is being created. The good π-stabilization on copper and gold carbenes, however, is due to two different factors: the high energy of the occupied *3d* orbitals on Cu(I) enhances π-back-donation into the ligand vacant orbitals[6c] whereas, for Au(I), relativistic effects prevail. Because of the contraction of the *6s* orbital, an expansion of the *5d* orbitals ensues from the increased shielding and subsequently leads to a more important overlap *S* between the metal and the ligands orbitals.

Finally, gold and copper do in fact differ due to the variation of their coordination number. Indeed the tendency of Au(I) complexes to adopt a bicoordinate linear geometry (and, in some rare cases, a T-shaped tricoordinate configuration)[36] significantly complicates the reaction scheme due to the restrictions of the coordination sphere. This exception within group 11 is also attributed to relativistic effects, which significantly increase the bending energy required to switch from a linear bicoordinate to a planar tricoordinate geometry. As a consequence the access to the productive carbocation $\mathbf{10^{Au}}$ from $\mathbf{3^{Au}}$ only occurs through a rather complicated energy profile. On the contrary the energetically accessible tri- and tetracoordinate configuration of Cu(I) and Ag(I) complexes allows much more flexibility.[37] Thus, $\mathbf{TS_{3-10}^{Cu}}$ and $\mathbf{TS_{3-10}^{Ag}}$ directly connect the ground-state metal−cyclopropane complexes $\mathbf{3^{Cu}}$ and $\mathbf{3^{Ag}}$ with the analogous carbocations $\mathbf{10^{Cu}}$ and $\mathbf{10^{Ag}}$ respectively.

CONCLUSIONS

Gas-phase studies have characterized the reactivity of IMes−coinage metal(I) complexes with dialkoxycyclopropane showing, in principle, two competing CID channels. We interpret the CID threshold curves in terms of a competition between dissociation, on the one hand, and rearrangement followed by dissociation, on the other. Fitting of the CID curves gives E_0 values, which, in the favorable cases, are consistent with expectations from potential energy surfaces computed with DFT methods. The density functional calculations indicate that there is a similar mechanism for carbene abstraction for all three metals. Bond Energy Decomposition Analysis showed that, for silver, the weak σ-interaction and more importantly the weak π-back-donation, which is crucial for the stabilization of the carbene moiety, render the carbene abstraction channel uncompetitive as compared to the dissociation channel. At the opposite end of the spectrum, the Au(I) carbene benefits from strong σ- and π-interactions leading to the observation of the carbene abstraction as the main channel. Studies carried out on group 11 elements using both gas-phase measurements and DFT calculations showed that, for comparable systems, such as NHC−metal carbenes, the trend Au > Cu > Ag is usually observed.

ASSOCIATED CONTENT

Supporting Information

Experiments details, ESI-MS spectra, threshold-CID measurements, NMR spectra, DFT absolutes energies and Cartesian coordinates. This material is available free of charge via the Internet at http://pubs.acs.org.

AUTHOR INFORMATION

Corresponding Author

peter.chen@org.chem.ethz.ch

Notes

The authors declare no competing financial interest.

ACKNOWLEDGMENTS

This manuscript is dedicated to Dr. Karin Halvorsen on the occasion of her 50th birthday. We thank the Swiss National Foundation for support of this work. L.B. thanks Dr. Erik P. A. Couzijn for helpful discussions.

REFERENCES

(1) (a) Armentrout, P.; Beauchamp, J. *J. Chem. Phys.* **1981**, *74*, 2819. (b) Armentrout, P. B.; Beauchamp, J. L. *J. Am. Chem. Soc.* **1981**, *103*, 6628. (c) Forbes, R. A.; Lech, L. M.; Freiser, B. S. *Int. J. Mass Spectrom. Ion Processes* **1987**, *77*, 107. (d) Georgiadis, R.; Armentrout, P. *Int. J.*

Mass Spectrom. Ion Processes **1989**, *89*, 227. (e) Sunderlin, L. S.; Armentrout, P. B. *J. Phys. Chem.* **1990**, *94*, 3589. (f) Simoes, J. M.; Beauchamp, J. *Chem. Rev.* **1990**, *90*, 629. (g) Chen, Y.-M.; Armentrout, P. *J. Phys. Chem.* **1995**, *99*, 11424. (h) Li, F.-X.; Armentrout, P. *J. Chem. Phys.* **2006**, *125*, 133114. (i) Li, F.; Hinton, C. S.; Citir, M.; Liu, F.; Armentrout, P. *J. Chem. Phys.* **2011**, *134*, 024310.

(2) (a) Batiste, L.; Fedorov, A.; Chen, P. *Chem. Commun.* **2010**, *46*, 3899. (b) Fedorov, A.; Batiste, L.; Bach, A.; Birney, D. M.; Chen, P. *J. Am. Chem. Soc.* **2011**, *133*, 12162.

(3) (a) Solorio-Alvarado, C. R.; Echavarren, A. M. *J. Am. Chem. Soc.* **2010**, *132*, 11881. (b) Solorio-Alvarado, C. R.; Wang, Y.; Echavarren, A. M. *J. Am. Chem. Soc.* **2011**, *133*, 11952.

(4) (a) Gassman, P. G.; Johnson, T. H. *J. Am. Chem. Soc.* **1976**, *98*, 6057. (b) Gassman, P. G.; Johnson, T. H. *J. Am. Chem. Soc.* **1976**, *98*, 6055. (c) Gassman, P. G.; Johnson, T. H. *J. Am. Chem. Soc.* **1976**, *98*, 6058.

(5) (a) Takaya, H.; Suzuki, T.; Kumagai, Y.; Hosoya, M.; Kawauchi, H.; Noyori, R. *J. Org. Chem.* **1981**, *46*, 2854. (b) Walczak, M. A. A.; Wipf, P. *J. Am. Chem. Soc.* **2008**, *130*, 6924.

(6) (a) Hertwig, R. H.; Koch, W.; Schröder, D.; Schwarz, H.; Hrušák, J.; Schwerdtfeger, P. *J. Phys. Chem.* **1996**, *100*, 12253. (b) Boehme, C.; Frenking, G. *Organometallics* **1998**, *17*, 5801. (c) Tai, H.-C.; Krossing, I.; Seth, M.; Deubel, D. V. *Organometallics* **2004**, *23*, 2343. (d) Hu, X.; Castro-Rodriguez, I.; Olsen, K.; Meyer, K. *Organometallics* **2004**, *23*, 755. (e) Lin, J. C. Y.; Huang, R. T. W.; Lee, C. S.; Bhattacharyya, A.; Hwang, W. S.; Lin, I. J. B. *Chem. Rev.* **2009**, *109*, 3561. (f) Fedorov, A.; Couzijn, E. P. A.; Nagornova, N. S.; Boyarkin, O. V.; Rizzo, T. R.; Chen, P. *J. Am. Chem. Soc.* **2010**, *132*, 13789.

(7) (a) Fructos, M. R.; Belderrain, T. R.; Nicasio, M. C.; Nolan, S. P.; Kaur, H.; Díaz-Requejo, M. M.; Pérez, P. J. *J. Am. Chem. Soc.* **2004**, *126*, 10846. (b) Díaz-Requejo, M. M.; Pérez, P. J. *J. Organomet. Chem.* **2005**, *690*, 5441. (c) Fructos, M. R.; Belderrain, T. R.; de Frémont, P.; Scott, N. M.; Nolan, S. P.; Díaz-Requejo, M. M.; Pérez, P. J. *Angew. Chem., Int. Ed.* **2005**, *44*, 5284. (d) Fructos, M. R.; de Frémont, P.; Nolan, S. P.; Díaz-Requejo, M. M.; Pérez, P. J. *Organometallics* **2006**, *25*, 2237. (e) Delgado-Rebollo, M.; Beltrán, Á.; Prieto, A.; Mar Díaz-Requejo, M.; Echavarren, A. M.; Pérez, P. J. *Eur. J. Inorg. Chem.* **2012**, *2012*, 1380. (f) Rivilla, I.; Sameera, W. M. C.; Alvarez, E.; Diaz-Requejo, M. M.; Maseras, F.; Perez, P. J. *Dalton Trans.* **2013**, *42*, 4132.

(8) Julian, R. R.; May, J. A.; Stoltz, B. M.; Beauchamp, J. L. *J. Am. Chem. Soc.* **2003**, *125*, 4478.

(9) (a) Hinderling, C.; Feichtinger, D.; Plattner, D. A.; Chen, P. *J. Am. Chem. Soc.* **1997**, *119*, 10793. (b) Gerdes, G.; Chen, P. *Organometallics* **2004**, *23*, 3031.

(10) (a) Couzijn, E. P. A.; Zocher, E.; Bach, A.; Chen, P. *Chem.—Eur. J.* **2010**, *16*, 5408. (b) Zocher, E. *Doct. Thesis ETH e-collection* **2008**, 78–85.

(11) (a) Moret, M.-E.; Serra, D.; Bach, A.; Chen, P. *Angew. Chem., Int. Ed.* **2010**, *49*, 2873. (b) Serra, D.; Moret, M.-E.; Chen, P. *J. Am. Chem. Soc.* **2011**, *133*, 8914.

(12) (a) Hinderling, C.; Adlhart, C.; Chen, P. *Angew. Chem., Int. Ed.* **1998**, *37*, 2685. (b) Adlhart, C.; Hinderling, C.; Baumann, H.; Chen, P. *J. Am. Chem. Soc.* **2000**, *122*, 8204. (c) Torker, S.; Merki, D.; Chen, P. *J. Am. Chem. Soc.* **2008**, *130*, 4808.

(13) In the case of the fragmentation product $\mathbf{5}^{\mathbf{M}}$, the authors recognize the existence of a debate focused on whether the active gold species should be described as a Au(I)-stabilized carbocation or a cationic Au carbene. Considering that other group 11 transition metals of similar reactivity are also used here, and that the resulting active species display different bonding patterns, we adopt the chemical representation of a metal–carbon double bond as a common formalism. We do not intend to favor a canonical cationic metal carbene as the preferred representation.

(14) Narancic, S.; Bach, A.; Chen, P. *J. Phys. Chem. A* **2007**, *111*, 7006.

(15) Frisch, M. J.; Trucks, G. W.; Schlegel, H. B.; Scuseria, G. E.; Robb, M. A.; Cheeseman, J. R.; Scalmani, G.; Barone, V.; Mennucci, B.; Petersson, G. A.; Nakatsuji, H.; Caricato, M.; Li, X.; Hratchian, H. P.; Izmaylov, A. F.; Bloino, J.; Zheng, G.; Sonnenberg, J. L.; Hada, M.; Ehara, M.; Toyota, K.; Fukuda, R.; Hasegawa, J.; Ishida, M.; Nakajima, T.; Honda, Y.; Kitao, O.; Nakai, H.; Vreven, T.; Montgomery, J. J. A.; Peralta, J. E.; Ogliaro, F.; Bearpark, M.; Heyd, J. J.; Brothers, E.; Kudin, K. N.; Staroverov, V. N.; Kobayashi, R.; Norm, J.; Raghavachari, K.; Rendell, A.; Burant, J. C.; Iyengar, S. S.; Tomasi, J.; Cossi, M.; Rega, N.; Millam, J. M.; Klene, M.; Knox, J. E.; Cross, J. B.; Bakken, V.; Adamo, C.; Jaramillo, J.; Gomperts, R.; Stratmann, R. E.; Yazyev, O.; Austin, A. J.; Cammi, R.; Pomelli, C.; Ochterski, J. W.; Martin, R. L.; Morokuma, K.; Zakrzewski, V. G.; Voth, G. A.; Salvador, P.; Dannenberg, J. J.; Dapprich, S.; Daniels, A. D.; Farkas, Ö.; Foresman, J. B.; Ortiz, J. V.; Cioslowski, J.; Fox, D. J. *Gaussian 09*; Gaussian Inc.: Wallingford, CT, 2009.

(16) Perdew, J. P.; Chevary, J.; Vosko, S.; Jackson, K. A.; Pederson, M. R.; Singh, D.; Fiolhais, C. *Phys. Rev. B* **1992**, *46*, 6671.

(17) Lynch, B. J.; Fast, P. L.; Harris, M.; Truhlar, D. G. *J. Phys. Chem. A* **2000**, *104*, 4811.

(18) Zhao, Y.; Truhlar, D. G. *Acc. Chem. Res.* **2008**, *41*, 157.

(19) Peterson, K. A.; Puzzarini, C. *Theor. Chem. Acc.* **2005**, *114*, 283.

(20) (a) Dunning, T. H., Jr. *J. Chem. Phys.* **1989**, *90*, 1007. (b) Peterson, K. A.; Woon, D. E.; Dunning, T. H., Jr. *J. Chem. Phys.* **1994**, *100*, 7410.

(21) (a) Mitoraj, M.; Michalak, A. *J. Mol. Model.* **2007**, *13*, 347. (b) Mitoraj, M. P.; Michalak, A.; Ziegler, T. *J. Chem. Theory Comput.* **2009**, *5*, 962.

(22) (a) Becke, A. D. *Phys. Rev. A* **1988**, *38*, 3098. (b) Perdew, J. P. *Phys. Rev. B* **1986**, *33*, 8822.

(23) (a) Te Velde, G.; Bickelhaupt, F. M.; Baerends, E. J.; Fonseca Guerra, C.; van Gisbergen, S. J. A.; Snijders, J. G.; Ziegler, T. *J. Comput. Chem.* **2001**, *22*, 931. (b) Guerra, C. F.; Snijders, J.; Te Velde, G.; Baerends, E. *Theor. Chem. Acc.* **1998**, *99*, 391.

(24) Xenon is heavier and more polarizable than Ar. For a given CID voltage offset (lab frame), the amount of energy transferred by Xe is greater than Ar, simply because of the kinematics. The center-of-mass energy (E_{CM}) is proportional to the mass of the collision gas (M_{gas}) and inversely proportional to the mass of the fragmenting ion (M_{ion}): $E_{CM} = E_{Lab}(M_{gas}/(M_{gas} + M_{ion})$. As a consequence, the same range of center-of-mass collision energies in the reactive cross section curves obtained with Ar are spread out over a larger range of voltage offsets than they would be for Xe. For the Au and Cu series, the appearance of a third channel occurs at low voltage offset when using Xe. A more spread-out range of voltage offset, for which only two channels were observed, could be obtained with Ar. This allows acquisition of a "denser" data set in the limited center-of-mass range which improves the quality of the fit. The cross sections for Au and Cu provided in Figure 2 were acquired using Ar.

(25) $\mathbf{TS}_{3-8}^{\mathbf{Au}}$ and $\mathbf{TS}_{8-9}^{\mathbf{Au}}$ were not considered for further study, since they lie at similar energy and involve the same type of chemistry as $\mathbf{TS}_{9-10}^{\mathbf{Au}}$ ($\mathbf{TS}_{3-8}^{\mathbf{Au}}$ corresponds to the M–O bond elongation and the ring opening of the three-membered ring providing $\mathbf{8}^{\mathbf{Au}}$, $\mathbf{TS}_{8-9}^{\mathbf{Au}}$ involves the ring closure and creation of a C–H agostic bond, and $\mathbf{TS}_{9-10}^{\mathbf{Au}}$ is characterized by the "productive" ring opening and the breakage of the C–H agostic bond leading to key-intermediate $\mathbf{10}^{\mathbf{Au}}$). Additionally the SI shows a very good geometry superimposition of $\mathbf{TS}_{8-9}^{\mathbf{Au}}$ and $\mathbf{TS}_{9-10}^{\mathbf{Au}}$. The $\mathbf{TS}_{9-10}^{\mathbf{Au}}$ provides hereby a good estimate of all three successive barriers.

(26) (a) Cirakovic, J.; Driver, T. G.; Woerpel, K. *J. Org. Chem.* **2004**, *69*, 4007. (b) Clark, T. B.; Woerpel, K. *Organometallics* **2005**, *24*, 6212. (c) Mayoral, J. A.; Rodríguez-Rodríguez, S.; Salvatella, L. *Eur. J. Org. Chem.* **2010**, *2010*, 1231. (d) Driver, T. G.; Woerpel, K. A. *J. Am. Chem. Soc.* **2004**, *126*, 9993.

(27) Grimme, S. *J. Comput. Chem.* **2006**, *27*, 1787.

(28) (a) Pérez-Galán, P.; Delpont, N.; Herrero-Gómez, E.; Maseras, F.; Echavarren, A. M. *Chem.—Eur. J.* **2010**, *16*, 5324. (b) Nakanishi, W.; Yamanaka, M.; Nakamura, E. *J. Am. Chem. Soc.* **2005**, *127*, 1446.

(29) (a) Nechaev, M. S.; Rayón, V. M.; Frenking, G. *J. Phys. Chem. A* **2004**, *108*, 3134. (b) Esterhuysen, C.; Frenking, G. *Chem.—Eur. J.* **2011**, *17*, 9944. (c) Dias, H. R.; Dash, C.; Yousufuddin, M.; Celik, M. A.; Frenking, G. *Inorg. Chem.* **2011**, *50*, 4253.

(30) von Hopffgarten, M.; Frenking, G. *WIREs Comput. Mol. Sci.* **2012**, *2*, 43.
(31) (a) Schwarz, H. *Angew. Chem., Int. Ed.* **2003**, *42*, 4442. (b) Heinemann, C.; Hertwig, R. H.; Wesendrup, R.; Koch, W.; Schwarz, H. *J. Am. Chem. Soc.* **1995**, *117*, 495. (c) Pitzer, K. S. *Acc. Chem. Res.* **1979**, *12*, 271. (d) Heß, B. A. *Ber. Bunsenges. Phys. Chem.* **1997**, *101*, 1. (e) Desclaux, J. P.; Pyykkö, P. *Chem. Phys. Lett.* **1976**, *39*, 300. (f) Schwerdtfeger, P. *Heteroatom. Chem.* **2002**, *13*, 578. (g) Pyykko, P.; Desclaux, J. P. *Acc. Chem. Res.* **1979**, *12*, 276.
(32) (a) Pyykkö, P. *Angew. Chem., Int. Ed.* **2004**, *43*, 4412. (b) Gorin, D. J.; Toste, F. D. *Nature* **2007**, *446*, 395. (c) Schwerdtfeger, P.; Hermann, H. L.; Schmidbaur, H. *Inorg. Chem.* **2003**, *42*, 1334.
(33) Schmidbaur, H.; Porter, K. In *Superacid chemistry*; Olah, G. A., Prakash, G. K. S., Molnár, À.; Sommer, J., Eds.; Wiley-Interscience: 2009; pp 291−308.
(34) (a) Saunders, M.; Vogel, P.; Hagen, E. L.; Rosenfeld, J. *Acc. Chem. Res.* **1973**, *6*, 53. (b) Koch, W.; Liu, B.; Schleyer, P. v. R. *J. Am. Chem. Soc.* **1989**, *111*, 3479. (c) Chiavarino, B.; Crestoni, M. E.; Fokin, A. A.; Fornarini, S. *Chem.—Eur. J.* **2001**, *7*, 2916.
(35) (a) Cheong, P. H.-Y.; Morganelli, P.; Luzung, M. R.; Houk, K. N.; Toste, F. D. *J. Am. Chem. Soc.* **2008**, *130*, 4517. (b) Seidel, G.; Lehmann, C. W.; Fürstner, A. *Angew. Chem.* **2010**, *122*, 8644. (c) Weber, D.; Jones, T. D.; Adduci, L. L.; Gagné, M. R. *Angew. Chem.* **2012**, *124*, 2502. (d) Weber, D.; Gagné, M. R. *Chem. Sci.* **2013**, *4*, 335. (e) Weber, D.; Tarselli, M. A.; Gagné, M. R. *Angew. Chem., Int. Ed.* **2009**, *48*, 5733.
(36) Schwerdtfeger, P.; Boyd, P. D. W.; Burrell, A. K.; Robinson, W. T.; Taylor, M. J. *Inorg. Chem.* **1990**, *29*, 3593.
(37) Carvajal, M. A.; Novoa, J. J.; Alvarez, S. *J. Am. Chem. Soc.* **2004**, *126*, 1465.